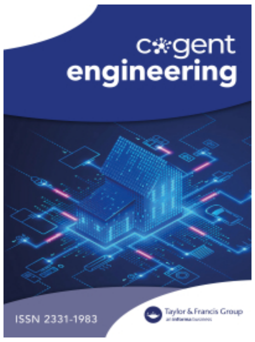

Cogent Engineering

ISSN: 2331-1916 (Online) Journal homepage: www.tandfonline.com/journals/oaen20

MHD nanofluid boundary layer flow through a stretching surface along with permeable media and activation energy

Anwar Shahid, Zhang Miao , Asad Mahmood , Muhammad Shafique & Adnan Khan

To cite this article: Anwar Shahid, Zhang Miao , Asad Mahmood , Muhammad Shafique & Adnan Khan (2025) MHD nanofluid boundary layer flow through a stretching surface along with permeable media and activation energy, Cogent Engineering, 12:1, 2582949, DOI: 10.1080/23311916.2025.2582949

To link to this article: https://doi.org/10.1080/23311916.2025.2582949

COGENT ENGINEERING
2025, VOL. 12, NO. 1, 2582949
https://doi.org/10.1080/23311916.2025.2582949

cogent

MECHANICAL ENGINEERING | RESEARCH ARTICLE

OPEN ACCESS

Check for updates

MHD nanofluid boundary layer flow through a stretching surface along with permeable media and activation energy

Anwar Shahid[a], Zhang Miao[a], Asad Mahmood[b], Muhammad Shafique[c] and Adnan Khan[d]

[a]School of Software, Quanzhou University of Information Engineering, Quanzhou, Fujian, P.R. China; [b]College of Science & Engineering, James Cook University, Townsville Campus, QLD, Australia; [c]Cyberspace Institute of Advanced Technology, Guangzhou University, Guangzhou, Guangdong, China; [d]College of Engineering, Shantou University, Shantou, Guangdong, China

ABSTRACT

A computational methodology is delineated to examine fluid concentration, velocity, and temperature as flow characteristics on the nanofluid boundary layer flowing through a porous stretchable subsurface along with permeable media and activation energy. An analysis of the movement, magnetohydrodynamic, and activation energy within the boundary layer is elucidated. The mathematical formulations of ordinary differentiation are obtained from the fundamental governing flow equations by employing similarity transformations. The resultant system of equations was solved numerically using the MATLAB bvp4c computational package. The computational outcomes are illustrated for dimensionless parameters with respect to the characteristics of fluid flow, concentration, and temperature. The computational findings indicate that an increase in the porous and magnetic field parameter reduces flow, while simultaneously enhancing temperature and concentration in this domain. The inclusion of nanofluid results in an augmentation of the thermal conductivity of the fluid flow. The conclusions drawn corroborate a notable concordance with prior research documented in the extant literature. The computational results and insights derived are extensively utilized in various engineering processes such as polymer drawing and extrusion, casting, hot rolling, and metal cooling. The incorporation of magnetic nanoparticles enhances the efficiency of thermal and mass transfer, thereby facilitating precision in oncological treatments, wastewater remediation, and processes that promote energy efficiency. The current investigation has broad implications across various sectors. These include optimizing energy efficiency in industrial processes, developing advanced cooling solutions, energy sectors, and renewable energy systems, and creating novel materials with tailored properties.

GRAPHICAL ABSTRACT

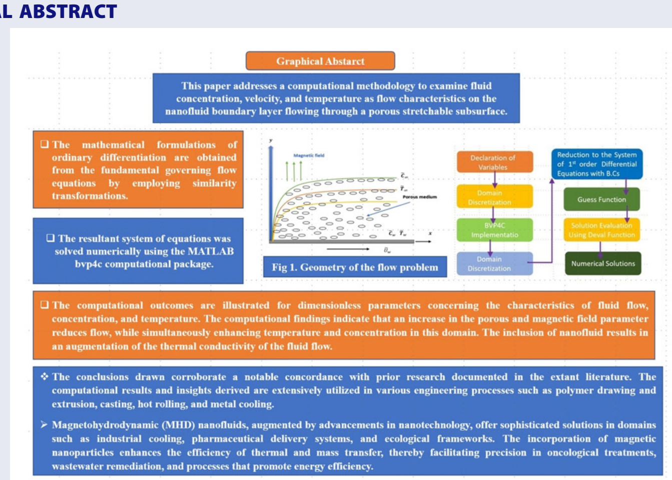

ARTICLE HISTORY
Received 11 January 2025
Revised 16 March 2025
Accepted 16 April 2025

KEYWORDS
Brownian Motion Parameter; MHD; Porous Media; Activation Energy; BVP4C Technique

SUBJECTS
Fluid Dynamics; Fluid Mechanics; Applied Mathematics

CONTACT Anwar Shahid anwarali@qzuie.edu.cn School of Software, Quanzhou University of Information Engineering, Quanzhou, 362000, Fujian, P.R. China

Nomenclature

$\tilde{u}, \tilde{v}$	Velocity components (ms^{-1})	ρ_f	Density of base fluid (Kgm^{-3})
ν_f	Kinematic viscosity of base fluid (m^2s^{-1})	σ_{nf}	Electrical conductivity
ν_{nf}	Kinematic viscosity of nanofluid (m^2s^{-1})	H_a	Hartmann number
$(\rho C_p)_{nf}$	Heat capacity of nanofluid	T_w	Wall Temperature
μ_{nf}	Viscosity of nanofluid (Nsm^{-2})	T_∞	Ambient Temperature
k_f	Thermal conductivity of base fluid ($Wm^{-1}K^{-1}$)	T	Temperature of fluid
B_0^2	Intensity of magnetic field	μ_f	Viscosity of base fluid (Nsm^{-2})
ρ_{nf}	Density of nanofluid (Kgm^{-3})	δ_1	Temperature difference
C_w, C_∞	Surface and ambient concentrations	P_r	Prandtl number
k^*	Mean absorption coefficient	m_1	Fitted constant
x, y	Coordinate axes	L_e	Lewis number
k_{nf}	Thermal conductivity of nanoparticles ($Wm^{-1}K^{-1}$)	β	Reaction rate parameter
		γ	Curvature parameter
K_p	Porosity parameter	σ^*	Stefan-Boltzmann constant
α_{nf}	Thermal diffusivity of nanofluid (m^2K^{-1})	$\Re_e$	Local Reynoled number
$\tilde{U}_w$	Stretching velocity (ms^{-1})	E_a	Coefficient of activation energy
E_1	Activation energy variable	$K_r{}^2$	Reaction rate
D_B	Diffusion coefficient of nanoparticles	N_t	Thermophoresis parameter
N_b	Brownian motion parameter		

1. Introduction

The fields of Engineering and industry rely heavily on the concept of stretching surfaces, a topic extensively explored in academic literature. The utilization of stretching sheets plays a pivotal role in various manufacturing processes. Such procedures include hot rolling for flow generation, rubber coat processing, glass blowing, fiber circling, polymer dyeing, and paper product manufacturing. The diverse applications of stretching sheets necessitate the reconsideration of different stretched velocities, i.e., linear, nonlinear, and exponential. In a seminal contribution, Crane [1] provided a precise solution for the flow resulting from the linear stretching of a sheet, a remarkable achievement in solving the Navier-Stokes equations. Subsequent research has expanded upon this work, investigating a wide array of physical properties, such as vertical suction/injection effects, heat and mass transfer along horizontal surfaces, and more. The influence of fluid motion on flat surfaces was scrutinized by Mukhopadhyay [2], while Mukhopadhyay and Reddy [3] studied the impact of Maxwell fluids on stretchable surfaces. Bhattacharyya et al. [4] explored variable viscosity effects in stagnation regions on stretching surfaces. Abbas et al. [5] extended this work by examining magnetohydrodynamics coupled with viscous flow on curved sheets, providing detailed analytical insights. Vajravelu and Mukhopadhyay [6] discussed the implications of fluid flow on body temperature, while Okechi et al. [7] investigated exponentially stretched sheets adopting a viscous liquid model. Ghosh and Nadeem et al. [8] numerically analyzed hybrid nanomaterial flows on curved sheets, and Gangadhar and Chamkha [9] studied the entropy impact on a couple-stress fluid with uniform heat generation. Abbas and Shatanawi [10] considered time-dependent flows on curved sheets using a micropolar fluid modeling, while Gangadhar et al. [11] numerically examined the thermal characteristics of hybrid nanofluids around rotating cylinders. Abbas and Shatanawi [12] explored the effects of exponential stretchable velocities subjected to chemically reactive second-grade fluids on curved sheets. Various researchers have contributed to the understanding of stretchable surfaces in different flow scenarios as evidenced by references [[13–15]].

Heat and mass transfer in the terrain of nanotechnology have performed a crucial part, owing to various instances associated with real-world issues. During the period of decay, traditional heat transfer mechanisms were utilized to elevate the system's temperature. This approach incurred significant costs and exhibited poor performance. A novel concept emerged involving the amalgamation of compact nano-particles with conventional fluid. The outcomes for such a concept offer greater benefits compared to the decay method. Among different particle sizes such as macro, micro, and nano-scaled, the latter has garnered more attention due to challenges in maintaining uniformity of the mixture or reducing pressure drop within the system. Because of their minute size and adjacency to the base fluid's molecules, these minuscule particles can establish highly reliable floating with nominal gravitational sedimentation occurring over protracted time intervals. Examples of this significance can be found in the cooling of electronic systems in modern electronics and the foundations of nuclear reactors. Heat transfer via nanofluid flow problems can be evaluated for different processes and equipment by utilizing heat conduction, which plays a crucial role in various heat transferal rate applications. Nanofluids, consisting of nanoparticles, have the potential to greatly enhance the characteristics of base fluids. The word "Nanofluid" was coined by Choi and Eastman [16], who highlighted the dispersion of nanoparticles within a standard fluid. Numerous researchers have adopted this concept and have witnessed exponential growth. Theoretical analyses have since been carried out to replicate the behaviors of nanofluids, resulting in the proposal of two models: homogeneous flows and dispersions modeling. Buongiorno [17] developed a theoretical model of nanofluids that omitted the influence of dispersion, particle diameter, and heat transport coefficient. Buongiorno's model elucidated the anomalous convective heat transferring augmentation in nanofluids, addressing the limitations of homogeneous and dispersion models. Akbar and Nadeem [18] extended Sutterby's ideas for a peristaltic model with an asymmetric media incline. The analytical outcomes have been advanced to illustrate the impact of slip. Ahmad et al. [19] analyzed the Sutterby fluid flow disputatiously along with the influences of chemical, radiation, and mixed convection on a constricted medium. Khan et al. [20] examined the effect of heterogeneous-homogeneous reactions on Sutterby fluid within a moving framework. The application of the Cattaneo–Christov models to the Sutterby fluid system was implemented to derive the principal findings. Mabood et al. [21] challenged the dynamic behavior of Sutterby fluid incorporating Fourier and Fick's laws on a revolving stretchable disk. Abdal et al. [22] examined nano-biofilms using Sutterby fluid on a stretching surface. Hanif et al. [23] characterized the Sutterby fluid model. Hussain et al. [24] investigated the impact of a ferromagnetic field and magnetic dipole on Sutterby fluid. Abdelsalam et al. [25] scrutinized the consequences of Sutterby fluid within the framework of an entropy model.

The study of magnetic field dynamics involves the interaction between a magnetic field and fluid mechanics, particularly with electrically conducting fluids. This dynamic interplay has attracted significant interest worldwide due to its broad applicability in areas such as astronomical physics, geophysics, and the dynamics of the earth's layers. Various engineering and industrial sectors, including plasma confinement and solar physics, also benefit from utilizing flow problems incorporating magnetic field characteristics, as numerous researchers acknowledge. Observations by experimental analysts reveal that the imposition of an extraneous magnetic field on fluid flow generates electric and magnetic fields. The predominant focus on the induced magnetic field over the induced electric field is attributed to the assumption of lesser magnetic Reynolds numbers. The presence of this generated magnetic field is crucial for the accurate representation of fluid flow dynamics. Several scholars have conducted initial investigations on electrically conducting fluid flows across different geometrical configurations, with select studies summarized for brevity. For instance, Daniel et al. [26] conducted entropy analysis on magnetic hydrodynamic nanomaterial fluid flowing considering radiative chemical reactions and viscous dissipations through numerical methods. They also explored MHD flow adopting the nanofluid model with mixed convection and partial slip conditions, among other variations. Mulinti and Pallavarapu [27] investigated the flow dynamics of an unsteady compressible magnetohydrodynamic fluid influenced by thermal radiation and situated within a porous subsurface, factoring in the presence of chemical reactions. The works of Wakif et al. [28], Reddy et al. [29], and Yahaya et al. [30] also contributed insights into the influence of MHD and nanofluids under diverse conditions. Recent scholarly discussions have centered on the magnetic hydrodynamic model under specific assumptions, as referenced in works [[31–35]].

Prior studies have not analyzed the MHD nanofluid flowing through a porous surface along with activation energy. The primary aspiration of disseminating this investigation endeavor is to elucidate the 2-D Navier-Stokes equation pertinent to Darcy-Brinkman flow induced by a stretchable subsurface, incorporating along with the MHD, activation energy, viscous and porous dissipation phenomena, which represents a significant knowledge gap. This study addresses this gap by analyzing the behavior of MHD nanofluid flowing with minimal alterations, the current results extrapolate the scenarios involving curved channel flow, specifically Couette flow in cylindrical geometries, as well as to parallel boundary layer dynamics. The governing non-linear partial differential equations have been reformulated into ordinary differential equations, subsequently resolved utilizing the BVP4C, which incorporates the BVP4C and

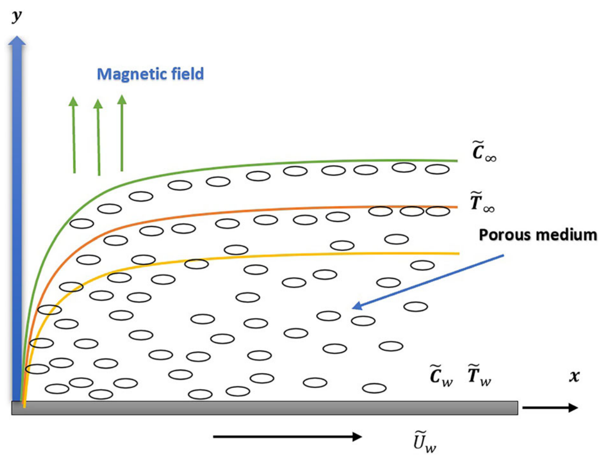

Figure 1. **Flow geometry.**

Newton-Raphson methodologies; both techniques have been employed to validate the accuracy of the results within the framework of the present investigation. The influence of various parametric quantities on velocity, concentration, and temperature has been thoroughly analyzed and explained. The outcomes of this study are intended to support and enhance further research initiatives and practical applications.

2. Mathematical modelling

This study examines a steady two-dimensional boundary layer of nanofluids flowing governed by magnetohydrodynamics (MHD) over a stretching surface within a porous medium. Assume that the flow is two-dimensional and steady, the fluid is incompressible and laminar, and the thermal equilibrium exists between the base fluid and nanoparticles. The plate extends along the $\boldsymbol{x}$-axis with a velocity denoted as "$\tilde{\boldsymbol{U}}_{\boldsymbol{w}}(\boldsymbol{x}) = \boldsymbol{a}_1\boldsymbol{x}$". Let $\tilde{\boldsymbol{U}}_{\boldsymbol{w}}, \tilde{\boldsymbol{T}}_{\boldsymbol{w}}$ and $\tilde{\boldsymbol{C}}_{\boldsymbol{w}}$ represent the fluid velocity, temperature, and nanoparticle concentration at the wall respectively. The temperature ($\tilde{\boldsymbol{T}}$) and nanoparticle concentration ($\tilde{\boldsymbol{C}}$) within the free stream, the fluids are established. The geometric representation of the investigated phenomenon is depicted in Figure 1. Utilizing the conventional presumptions and symbols associated with boundary layer flow [36], the fundamental conservation equations governing mass, momentum, energy, and concentration are articulated in assertions (1)-(5).

$$\frac{\partial \tilde{u}}{\partial x} = -\frac{\partial \tilde{v}}{\partial y}, \tag{1}$$

$$\tilde{u}\frac{\partial \tilde{u}}{\partial x} + \tilde{v}\frac{\partial \tilde{u}}{\partial y} = -\frac{1}{\rho_f}\frac{\partial p}{\partial x} + \frac{\mu_1}{\rho_f}\left\{\frac{\partial^2 \tilde{u}}{\partial x^2} + \frac{\partial^2 \tilde{u}}{\partial y^2}\right\} - \frac{\sigma B_0^2 \tilde{u}}{\rho_f} - \frac{\nu \tilde{u}}{k}, \tag{2}$$

$$\tilde{u}\frac{\partial \tilde{v}}{\partial x} + \tilde{v}\frac{\partial \tilde{v}}{\partial y} = -\frac{1}{\rho_f}\frac{\partial p}{\partial y} + \frac{\mu_1}{\rho_f}\left\{\frac{\partial^2 \tilde{v}}{\partial x^2} + \frac{\partial^2 v}{\partial y^2}\right\} - \frac{\sigma B_0^2 \tilde{v}}{\rho_f} - \frac{\nu \tilde{v}}{k}, \tag{3}$$

$$\tilde{u}\frac{\partial \tilde{T}}{\partial x} + \tilde{v}\frac{\partial \tilde{T}}{\partial y} - \alpha_1\left\{\frac{\partial^2 \tilde{T}}{\partial x^2} + \frac{\partial^2 \tilde{T}}{\partial y^2}\right\} = \tau\left\{\frac{D_B}{\Delta \tilde{C}}\left[\frac{\partial \tilde{T}}{\partial x}\frac{\partial \tilde{C}}{\partial x} + \frac{\partial \tilde{T}}{\partial y}\frac{\partial \tilde{C}}{\partial y}\right] + \frac{D_{\tilde{T}}}{\tilde{T}_\infty}\left[\left(\frac{\partial \tilde{T}}{\partial x}\right)^2 + \left(\frac{\partial \tilde{T}}{\partial y}\right)^2\right]\right\}, \tag{4}$$

$$\tilde{u}\frac{\partial \tilde{C}}{\partial x} + \tilde{v}\frac{\partial \tilde{C}}{\partial y} = D_B\left\{\frac{\partial^2 \tilde{C}}{\partial x^2} + \frac{\partial^2 \tilde{C}}{\partial y^2}\right\} + \frac{D_{\tilde{T}}}{\tilde{T}_\infty}\left\{\frac{\partial^2 \tilde{T}}{\partial x^2} + \frac{\partial^2 \tilde{T}}{\partial y^2}\right\} - K_r{}^2\left[\frac{\tilde{T}}{\tilde{T}_\infty}\right]^{m_1} e^{-\left(\frac{E_a}{K\tilde{T}}\right)}\left(\tilde{C} - \tilde{C}_\infty\right), \tag{5}$$

together with the corresponding boundary conditions

$$\tilde{u} = \tilde{U}_w(x) = a_1 x, \tilde{v} = 0, \tilde{T} = \tilde{T}_w, \tilde{C} = \tilde{C}_w \text{ at } y = 0, \tag{6}$$

$$\tilde{u}=0,\tilde{v}=0,\tilde{T}=\tilde{T}_{\infty},\tilde{C}=\tilde{C}_{\infty}\text{ as }y\rightarrow\infty. \tag{7}$$

In these expressions $\tilde{u}$ and $\tilde{v}$ denote the velocities along the x and y-axes correspondingly, ρ_f stands for fluid density, (k) refers to the thermal conductivity, while (p) denotes the fluid pressure, (D_B) is the Brownian diffusion coefficient, ($D_{\tilde{T}}$) indicates the thermophoretic diffusion coefficient, μ_1 represents viscosity, and nanoparticle density is represented by ρ_p, respectively. ($\tilde{T}$) indicates the temperature of the fluid, ($\tilde{T}_{\infty}$) denotes the free stream temperature. Furthermore, the effective heat capacity is defined as $\tau=(\rho c)_p/(\rho c)_f$, where the thermal capacity of the nanoparticles is $(\rho c)_p$, and that of the nanofluid is $(\rho c)_f$.

Where the stream function "ψ"is written as:

$$\tilde{u}=\frac{\partial\psi}{\partial y}=,\tilde{v}=-\frac{\partial\psi}{\partial x}, \tag{8}$$

Considering the non-dimensional transformations below:

$$\tilde{u}=a_1\tilde{x}\mathrm{F}^{'}(\eta),\eta=\tilde{y}\sqrt{\frac{a_1}{\nu}},\tilde{v}=-\sqrt{a_1\nu}\mathrm{F}(\eta),\theta(\eta)=\frac{\tilde{T}-\tilde{T}_{\infty}}{\tilde{T}_w-\tilde{T}_{\infty}},\phi(\eta)=\frac{\tilde{C}-\tilde{C}_{\infty}}{\tilde{C}_w-\tilde{C}_{\infty}}. \tag{9}$$

In consideration of the similarity transformations (9), equation (1) is satisfied evenly while equations (2)–(5) are simplified to the subsequent form.

$$\mathrm{F}'''+\mathrm{F}\mathrm{F}''-\mathrm{F}^{'2}-H_a\mathrm{F}^{'}-K_{\boldsymbol{p}}\mathrm{F}^{'}=0, \tag{11}$$

$$\frac{1}{P_r}\theta''+\mathrm{F}\theta^{'}+N_b\phi^{'}\theta^{'}+N_t\theta^{'2}=0, \tag{12}$$

$$\phi''+Le\mathrm{F}\phi^{'}+\frac{\mathrm{N}_t}{N_b}\theta''-Le\sigma_1[1+\delta_1\theta]^{m_1}\exp\left(\frac{-E}{1+\delta_1\theta}\right)\phi=0, \tag{13}$$

in conjunction with the relevant boundary conditions:

$$\mathrm{F}^{'}=1,\mathrm{F}=0,\theta=1,\phi=1\text{ at }\eta=0, \tag{14}$$

$$\mathrm{F}^{'}=0,\theta=0,\phi=0\text{ as }\eta=\infty. \tag{15}$$

Where H_a symbolizes the magnetic parameter, β_D symbolizes the porous parameter, P_r symbolizes the Prandtl number, N_t symbolizes the thermophoresis parameter, N_b symbolizes the Brownian motion parameter and L_e symbolizes the Lewis number, E_1 activation energy variable, E_a Coefficient of activation energy, $K_r{}^2$ Reaction rate, δ_1 Temperature difference, σ_1 denotes the chemical reactive factor, are as follows:

$$H_a=\frac{\sigma B_0^2}{\rho_1 a_1}=,K_p=\frac{\nu}{ka_1},P_r=\frac{\nu}{\alpha},N_t=\frac{\tau D_{\tilde{T}}\left(\tilde{T}_w-\tilde{T}_{\infty}\right)}{\nu_f\tilde{T}_{\infty}},$$

$$N_b=\frac{\tau D_B}{\Delta\tilde{C}}\frac{\left(\tilde{C}_w-\tilde{C}_{\infty}\right)}{\nu_f\tilde{T}_{\infty}},E=\frac{E_a}{K_0\tilde{T}_{\infty}},\sigma_1=\frac{K_r{}^2}{a_1},\delta_1=\frac{\tilde{T}_w-\tilde{T}_{\infty}}{\tilde{T}_{\infty}},L_e=\frac{\nu}{D_B}.$$

The expressions for "$\boldsymbol{C_{fx}},\boldsymbol{N_x},\boldsymbol{Sh_x}$" are obtained as

$$C_{fx}=-\frac{\tau_w}{\rho_1\tilde{U}_w{}^2},N_x=-\frac{xq_w}{k(T_w-T_{\infty})}\bigg|_{y=0},S_h=-\frac{xq_m}{D_B(C_w-C_{\infty})}\bigg|_{y=0} \tag{16}$$

And

$$\tau_w=-\mu_1\left[\frac{\partial\tilde{u}}{\partial y}\right]_{y=0},q_w=-k\frac{\partial\tilde{T}}{\partial y}\bigg|_{y=0},q_m=-D_B\frac{\partial\tilde{C}}{\partial y}\bigg|_{y=0} \tag{17}$$

Here, μ_1 signifies the dynamic viscosity of nanofluid, while k signifies the thermal conductivity of nanofluid.

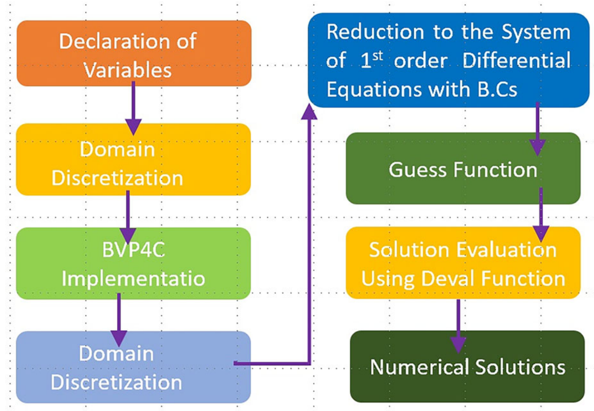

Figure 2. Process flow diagram for generating numerical results.

The physical quantity of interest such as skin friction coefficient, etc., "$\boldsymbol{C_{fx}, N_x, Sh_x}$" are given by

$$-\sqrt{\Re_e}C_{fx} = \left[\mathrm{F}''(\eta)\right]_{\eta=0}, \sqrt{\Re_e}N_x = \left[-\theta'(\eta),\right]_{\eta=0}, \sqrt{\Re_e}Sh_x = \left[-\phi'(\eta)\right]_{\eta=0} \tag{18}$$

where $\Re_e = \frac{a_1 x^2}{\nu_f}$ is the local Reynolds number predicated upon the velocity of stretching $\tilde{U}_w(x)$.

3. Numerical analysis governing flow phenomenon

The BVP4C Technique is applied to address the nonlinear coupled differential equations (11)-(13) which are governed by the boundary conditions (14) and (15). Assuming

$$\mathrm{F} = Z_1, \mathrm{F}' = Z_2, \mathrm{F}'' = Z_3, \theta = Z_4, \theta' = Z_5, \phi = Z_6, \phi' = Z_7, \tag{19}$$

Consequently, we get

$$Z_3{}' = Z_2{}^2 + H_a Z_2 + \beta_D Z_2 - Z_1 Z_3, \tag{20}$$

$$Z_5{}' = -P_r\left(Z_1 Z_5 + N_b Z_7 Z_5 + N_t Z_5{}^2\right), \tag{21}$$

$$Z_7{}' = -Le\left(Z_1 Z_7 + \frac{N_t}{N_b} Z_5{}' - Le\sigma_1[1+\delta_1\theta]^{m_1} \exp\left(\frac{-E}{1+\delta_1\theta}\right) Z_6\right), \tag{22}$$

The associated boundary conditions adjust correspondingly

$$Z_2 = 1, Z_1 = 0, Z_4 = 1, Z_6 = 1 \text{ at } \eta = 0, \tag{23}$$

$$Z_2 = 0, Z_4 = 0, Z_6 = 0 \text{ as } \eta = \infty. \tag{24}$$

The solution procedure for generating numerical results is displayed in Figure 2. The choice of BVP4C over other numerical schemes like finite element or finite difference methods is justified by its accuracy, efficiency, and relative simplicity, especially when dealing with highly nonlinear ODEs. Its adaptive mesh selection, user-friendly interface, and robust handling of nonlinearities make it a valuable tool for solving boundary value problems in various scientific and engineering applications. While FEM and FDM have their strengths, BVP4C offers a balanced approach that often provides a more straightforward and computationally efficient solution.

4. Results and discussion

This section elucidates the graphical representations and numerical findings of the BVP4C concerning an array of physical parameters. This section presents an analysis regarding the variation of multiple emerging parameters associated with velocity, temperature, and concentration profiles. The numerical depiction and scrutiny of these variations are carried out.

Table 1. Numerical comparability of "N_x, Sh_x" with antecedent results by stipulating $H = \beta_D = \sigma_1 = E = 0$, $N_b = 0.1$, $P_r = L_e = 10$.

N_t	W. A. Khan and I. Pop [37]	Current results for N_x	W. A. Khan and I. Pop [37]	Current results for Sh_x
0.1	0.9524	0.9522	2.1294	2.1295
0.2	0.6932	0.6933	2.2740	2.2742
0.3	0.5201	0.5201	2.5286	2.5287

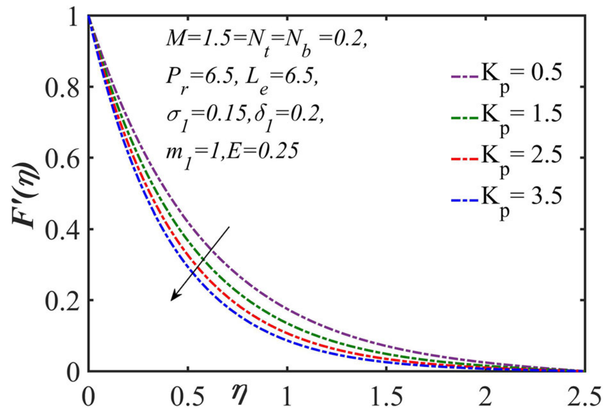

Figure 3. Aftereffect of K_p over velocity profile.

4.1. Tabular results:

To evaluate the precision of the numerical methodology employed, the results are juxtaposed with the extant literature provided by Khan and Pop [37]. It has been noted that the results yielded by the BVP4C method exhibit a higher degree of accuracy as delineated in Table 1. While the BVP4C method is known for its high accuracy in solving boundary value problems, discrepancies can arise when comparing its results with other numerical methods. These discrepancies can be attributed to factors such as approximations, round-off errors, truncation errors, discretization, convergence criteria, and model simplifications.

To illustrate potential discrepancies, consider a scenario where the skin friction coefficient is calculated using both the BVP4C method and a finite difference scheme. Suppose that across a specific set of parameters, the BVP4C method yields the Nusselt number coefficient of 0.0144, while the finite difference method gives a value of 0.0143. The percentage deviation can be calculated as:

$$\text{Percentage Deviation} = \frac{\|0.6933 - 0.6932\|}{0.6933} \times 100 \approx 0.0144\%$$

This small deviation highlights the level of agreement between the two methods. In some cases, deviations might be larger due to the abovementioned factors, such as differences in truncation errors or model simplifications.

4.2. Graphical results

Figure 3 illustrates that an escalation in H_a causes a decline in "$\mathrm{F}^{'}$" as a consequence of the prevalence of the Lorentz force, which enhances viscous forces. The impact of β_D on the magnitude of velocity is demonstrated in Figure 4, indicating that the decrease in velocity "$\mathrm{F}^{'}$" is associated with the augmentation of the momentum boundary layer thickness. The permeable parameter $\beta_D = \frac{\nu}{ka_1}$ in equation (9) signifies the Darcian term $-\beta_D \mathrm{F}^{'}$" and inversely affects the medium's permeability, consequently influencing the velocity profile "$\mathrm{F}^{'}$". As β_D increases, there is a reduction in permeability, resulting in heightened resistance from solid fibers present in the viscoelastic fluid and ultimately leading to a deceleration in "$\mathrm{F}^{'}$". The permeability is also treated as a resistive force, and this causes a significant deceleration in the velocity distribution for the flow within a permeable medium. This also favors retarding the thickness of the profile throughout. The effectiveness of "H_a" over the velocity profile in Figure 3 indicates a significant deceleration in velocity with an increase in H_a due to the emergence of a resistive force called the

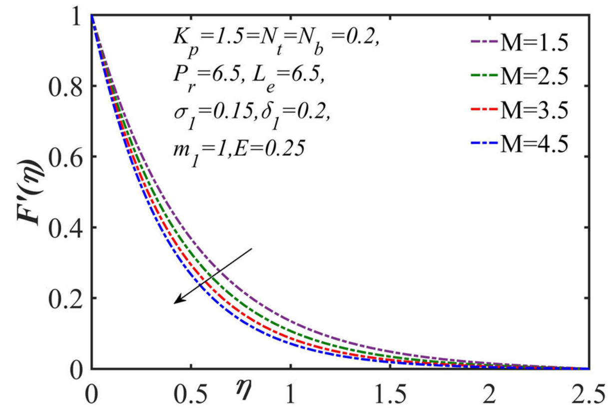

Figure 4. Aftereffect of *M* over velocity profile.

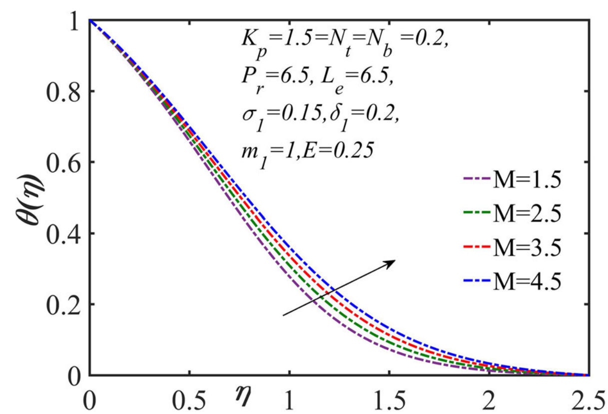

Figure 5. Effectiveness of *M* on θ (η).

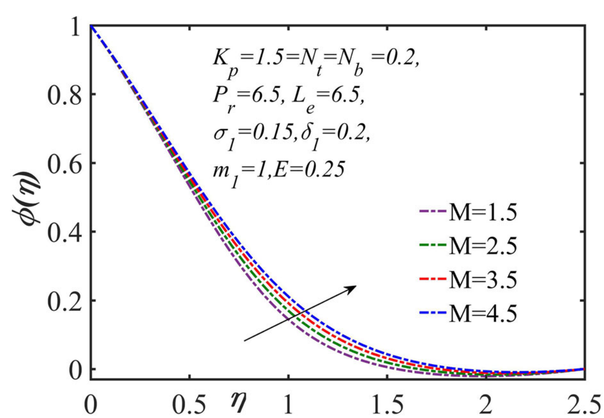

Figure 6. Aftereffect of *M* on concentration profile.

Lorentz force, resulting in a reduction in velocity overshooting and thickening of the momentum boundary layer.

The relationship between the temperature function and the Hartmann number displays some variability, as depicted in Figures 5-6. A discernible enhancement in the thermal and concentration profiles concomitant with an increase in "H_a" has been documented, as well as a rise in thermal boundary thickness. Furthermore, the influence of the magnetic field, in conjunction with the thermophysical characteristics of the nanofluid, engenders a thermal boundary layer wherein temperature gradients are accentuated as a result of differential thermal conductivity. The interaction among these factors results in an augmentation of the thermal boundary layer thickness as the concentration of nanoparticles is elevated,

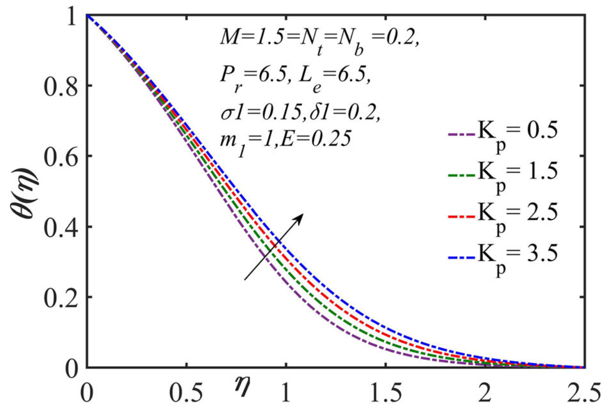

Figure 7. Effectiveness of K_p on $\theta\ (\eta)$.

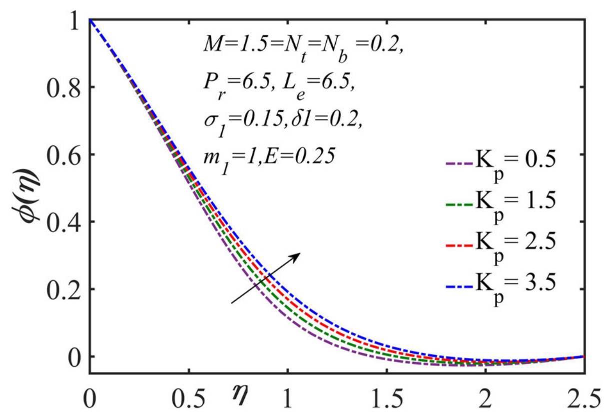

Figure 8. Aftereffect of K_P on concentration profile.

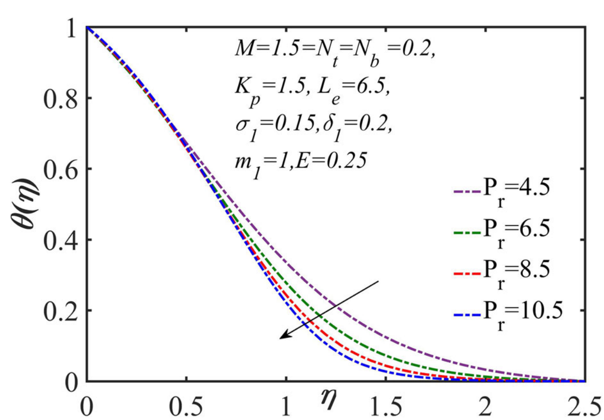

Figure 9. Impact of P_r over temperature magnitude.

subsequently improving the thermal transfer efficiency of the fluid. The augmentation of the porous parameter (K_p) results in a reduction of fluid flow, while temperature and concentration increase within this specific domain as demonstrated by Figures 7-8. From Figure 9, it can be observed that an elevation in the Prandtl number "P_r", ensuing a diminution in the fluid temperature, $\theta(\eta)$, and simultaneously diminishes the thickness of the thermal boundary layer, attributable to the actuality that an upturn in P_r leads to a reduction in thermal conductivity. Consequently, a fluid characterized by a higher "P_r" exhibits a diminished thermal boundary layer thickness. Physically, the Prandtl number relates the relative effectiveness of momentum and heat transport in a fluid. A high Prandtl number indicates that momentum diffusivity is more dominant than thermal diffusivity, meaning that momentum transfer occurs more effectively than heat transfer. Conversely, a low Prandtl number signifies that thermal diffusivity

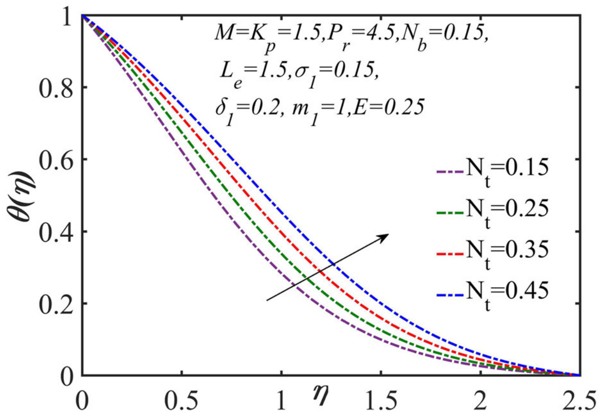

Figure 10. Aftereffect of N_t on temperature distribution.

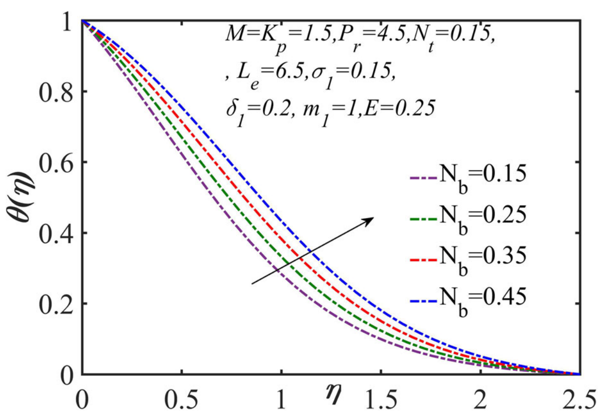

Figure 11. Aftereffect of N_b on temperature magnitude.

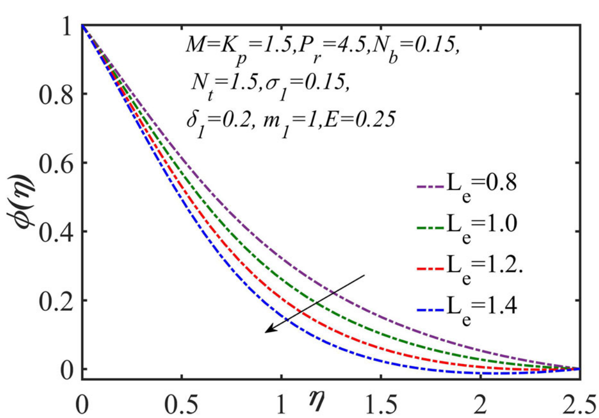

Figure 12. Aftereffect of L_e on $\phi\ (\eta)$.

dominates, implying that heat transfer is more efficient than momentum transfer. The Prandtl number is a fluid property that depends on temperature and pressure but is independent of the flow geometry. Figure 10 elucidates the behavior of the thermal profile across an extensive range of thermophoresis factors (N_t). As N_t escalates, the surface from which heat is extracted does so at an accelerated rate due to the thermophoretic force generated by the prevailing temperature gradient. The effect of N_b for flow field is observed. In Figure 11, the upsurging in N_b yields a more uniform temperature distribution.

The behavior of the Lewis number (L_e) about concentration is presented in Figure 12, indicating that as (L_e) values rise, the concentration curve tends to flatten out. As the magnitude of concentration increases with elevated values of (N_t), it conversely diminishes when larger values of (N_b) are considered as presented in Figures 13-14. This phenomenon can be attributed to the enhancement of thermal

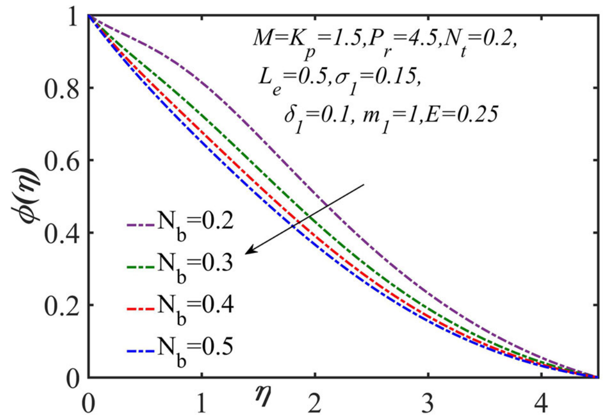

Figure 13. Aftereffect of N_t on $\phi\ (\eta)$.

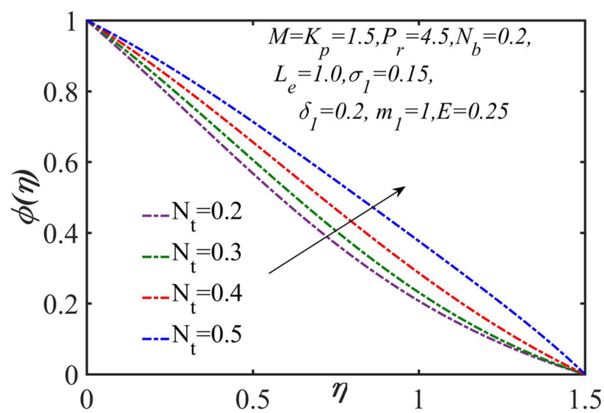

Figure 14. Aftereffect of N_b on $\phi\ (\eta)$.

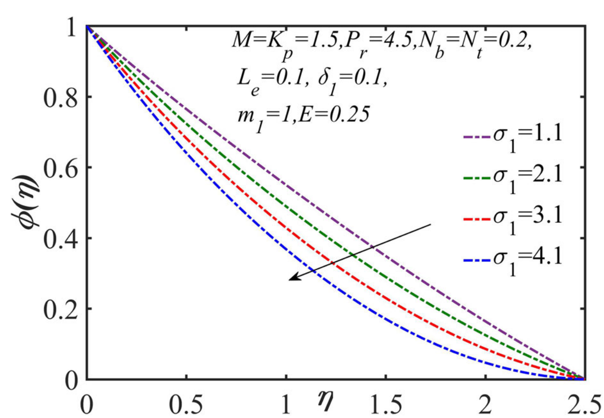

Figure 15. Aftereffect of σ_1 on $\phi\ (\eta)$.

transfer and the distribution of nanoparticles. The Brownian motion directly correlates with temperature; consequently, nanoparticles acquire energy. Hence, it escalates with a temperature rise. Conversely, the inverse relationship between concentration and the Brownian motion parameter is attributed to the thinning of the boundary layer, as the stochastic movement of fluid particles diminishes concentration. The ramifications of the chemical reaction constant (σ_1) and the parametric variable of activation energy (E) are illustrated in Figures 15-16, which demonstrates that ϕ declines with increasing values of σ_1, whilst it ascends with the augmentation of the numerical value of E.

Moreover, phenomena such as Brownian motion and thermophoresis play a pivotal role in the dispersion of nanoparticles within a fluidic medium, thereby impacting both thermal conductivity and viscosity. The correlation between concentration variations and physical properties is of paramount

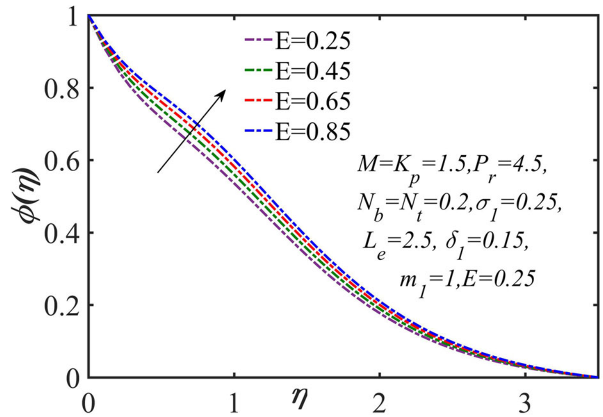

Figure 16. Aftereffect of E on ϕ (η).

importance for the engineering of systems in which the efficient administration of nanoscale particles is necessary for the optimization of processes such as pharmaceutical delivery or improved thermal transfer.

5. Conclusions

The analysis of the boundary layer nanofluid flowing past a permeable stretched surface situated within a porous medium and activation energy has been conducted in the present study. Similarity transformations have been employed to translate the conservative representation of momentum, energy, and nanoparticle concentration into ODEs. The BVP4C methodology is applied to the governing non-linear equations of the flow, alongside their corresponding boundary conditions via MATLAB, and the resultant findings are presented through graphical representations; additionally, a comparative analysis of the results obtained with those from prior studies is provided. The salient findings of the present investigation are:

1. The velocity experiences a decline through the augmentation of numerical variables associated with permeability "β_D" and the magnetic parameter "H_a", concurrently enhancing the thickening of the momentum boundary layer situated above the extended plate. Meanwhile, temperature and concentration profiles increase within this specific domain.
2. An elevation in the Prandtl number "P_r", arises in a downturn in the fluid temperature $\theta(\eta)$ as well as the thermal boundary layer.
3. As the parametric quantities N_t and N_b escalate, temperature distributions enhance, and so does thermal boundary thickness.
4. As (L_e) and (N_t) values rise, the concentration curve tends to surge out. Whereas less pronounced concentration profiles with decreasing (N_b) due to the creation of a thinner border layer.
5. The magnitudes of concentration exhibit a reduction in velocity with an increase in the numerical value of σ_1, while their graphical representations ascend with an elevation in E.
6. The BVP4C methodology offers a comprehensive framework for resolving practical issues across a multitude of disciplines, including, but not limited to, energy systems, industrial manufacturing, environmental engineering, and biomedicine.
7. Magnetohydrodynamic (MHD) nanofluids, augmented by advancements in nanotechnology, offer sophisticated solutions in domains such as industrial cooling, pharmaceutical delivery systems, and ecological frameworks. The incorporation of magnetic nanoparticles enhances the efficiency of thermal and mass transfer, thereby facilitating precision in oncological treatments, wastewater remediation, and processes that promote energy efficiency. It holds immense potential for innovation across multiple engineering disciplines, paving the way for sustainable and efficient technological solutions.

The major findings show that the presence of a magnetic field leads to a distinct reduction in fluid velocity, while the temperature increases, indicating enhanced heat transfer behavior within the nanofluid. This research enhances the understanding of nanofluid dynamics and provides insights into improving thermal management systems in various engineering applications, highlighting the importance of optimizing these fluids for increased efficacy. It contributes significantly to the design and implementation of more efficient heat transfer systems, particularly in sectors where precise thermal control is critical, such as electronic cooling and power generation.

The future research should focus on understanding the impacts of non-uniform nanoparticle distributions and the dynamics of nanofluid stability in various operating environments.

Acknowledgments

Anwar Shahid [1, *]: Conceptualization, methodology, investigation, software, validation Zhang Miao[1]: formal analysis, software Asad Mahmood[2]: Conceptualization, investigation, writing review, and editing Muhammad Shafique[3]: writing-original draft preparation Adnan Khan[4]: writing-original draft preparation "All authors have read and approved the final version of the manuscript"

Author's contribution

CRediT: **Anwar Shahid**: Conceptualization, Methodology, Software, Validation; **Zhang Miao**: Formal analysis, Software, Supervision; **Asad Mahmood**: Conceptualization, Formal analysis; **Muhammad Shafique**: Supervision, Writing – original draft; **Adnan Khan**: Writing – original draft, Writing – review & editing.

Disclosure statement

None of the authors have any conflicts of interest concerning this study to disclose.

Funding

This research received no external funding.

ORCID

Anwar Shahid http://orcid.org/0000-0003-2702-6457
Muhammad Shafique http://orcid.org/0000-0001-9929-3744

Availability of data and materials

The datasets generated and/or analyzed during the current study are available from the corresponding author upon reasonable request. All relevant data supporting the findings of this study, including any supplementary materials, are provided in the manuscript and supplementary files. Any additional materials used during the study can be made available upon request to ensure transparency and replicability.

References

1. Crane, L. J. (1970). Flow past a stretching plate. *Zeitschrift Für Angewandte Mathematik Und Physik ZAMP*, *21*(4), 645–647. https://doi.org/10.1007/BF01587695
2. Mukhopadhyay, S. (2011). Heat transfer in a moving fluid over a moving non-isothermal flat surface. *Chinese Physics Letters*, *28*(12)Article, 124706. https://doi.org/10.1088/0256-307X/28/12/124706
3. Mukhopadhyay, S., & Reddy Gorla, R. S. (2012). Unsteady MHD boundary layer flow of an upper convected Maxwell fluid past a stretching sheet with first order constructive/destructive chemical reaction. *J. Nav. Architect. Mar. Eng*, *9*(2), 123–133.
4. Bhattacharyya, K., Mukhopadhyay, S., & Layek, G. (2012). Effects of partial slip on boundary layer stagnation-point flow and heat transfer towards a stretching sheet with temperature dependent fluid viscosity. *Acta Technica CSAV*, *57*(2), 183–195.
5. Abbas, Z., Naveed, M., & Sajid, M. (2013). Heat transfer analysis for stretching flow over a curved surface with magnetic field. *Journal of Engineering Thermophysics*, *22*(4), 337–345. https://doi.org/10.1134/S1810232813040061

6. Vajravelu, K., & Mukhopadhyay, S. (2015). Fluid Flow, Heat and Mass Transfer at Bodies of Different Shapes. *Numerical Solutions*., Academic Press.
7. Okechi, N. F., Jalil, M., & Asghar, S. (2017). Flow of viscous fluid along an exponentially stretching curved surface. *Results in Physics*, *7*, 2851–2854. https://doi.org/10.1016/j.rinp.2017.07.059
8. Nadeem, S., Abbas, N., & Malik, M. Y. (2020). Inspection of hybrid based nanofluid flow over a curved surface. *Computer Methods and Programs in Biomedicine*, *189*Article, 105193. https://doi.org/10.1016/j.cmpb.2019.105193
9. K, G., D, N. B., M, V. S. R., & Chamkha, A. J. (2021). Entropy minimization on magnetized Boussinesq couple stress fluid with non-uniform heat generation. *Physica Scripta*, *96*(9)Article, 095205. https://doi.org/10.1088/1402-4896/ac03de
10. Abbas, N., & Shatanawi, W. (2022). Theoretical survey of time-dependent micropolar nanofluid flow over a linear curved stretching surface,. *Symmetry*, *14*(8), 1629. https://doi.org/10.3390/sym14081629
11. Gangadhar, K., Mary Victoria, E., & Chamkha, A. J. (2022). Hydrothermal features in the swirling flow of radiated graphene–Fe3O4 hybrid nanofluids through a rotating cylinder with exponential space-dependent heat generation. Waves Random Complex Media. 1–24.
12. Abbas, N., Ali, M., & Shatanawi, W. (2023). Chemical reactive second-grade nanofluid flow past an exponential curved stretching surface: Numerically. *Int. J. Mod. Phys, B* Article, 2450026.
13. Ullah, S., Ullah, I., Ali, A., Shah, K., & Abdeljawad, T. (2024). Investigation of cross-diffusion effect on radiative Jeffery-Hamel flow in convergent/divergent stretchable channel with Lorentz force and Joule heating. *Alexandria Engineering Journal*, *86*, 289–297. https://doi.org/10.1016/j.aej.2023.11.054
14. Shahid, A., Huang, H., Bhatti, M. M., Zhang, L., & Ellahi, R. (2020). Numerical investigation on the swimming of gyrotactic microorganisms in nanofluids through porous medium over a stretched surface. *Mathematics*, *8*(3), 380. https://doi.org/10.3390/math8030380
15. Shahid, A., Wei, W., Bhatti, M. M., Bég, O. A., & Bég, T. A. (2023). Mixed convection Casson polymeric flow from a nonlinear stretching surface with radiative flux and non-Fourier thermal relaxation effects: Computation with CSNIS, ZAMM. - *Journal of Applied Mathematics and Mechanics*, *103*(10), 1–15. https://doi.org/10.1002/zamm.202200519
16. Choi, S. U., & Eastman, J. A. (1995)., Enhancing Thermal Conductivity of Fluids with Nanoparticles (No. ANL/MSD/CP-84938; CONF-951135-29), Argonne National Lab. (ANL), Argonne, IL (United States
17. Buongiorno, J. (2006). Convective transport in nanofluids. *Journal of Heat Transfer*, *128*(3), 240–250. https://doi.org/10.1115/1.2150834
18. Akbar, N. S., & Nadeem, S. (2014). Convective heat transfer of a Sutterby fluid in an inclined asymmetric channel with partial slip, *Heat Tran*. *Res*, *45*(3), 219–240.
19. Ahmad, S., Farooq, M., Javed, M., & Anjum, A. (2018). Double stratification effects in chemically reactive squeezed Sutterby fluid flow with thermal radiation and mixed convection. *Results in Physics*, *8*, 1250–1259. https://doi.org/10.1016/j.rinp.2018.01.043
20. Khan, M. I., Qayyum, S., Hayat, T., & Alsaedi, A. (2019). Stratified flow of Sutterby fluid with homogeneous-heterogeneous reactions and Cattaneo-Christov heat flux. *International Journal of Numerical Methods for Heat & Fluid Flow*, *29*(8), 2977–2992. https://doi.org/10.1108/HFF-12-2018-0762
21. Mabood, F., Mackolil, J., Mahanthesh, B. S. E. P., Rauf, A., & Shehzad, S. A. (2021). Dynamics of Sutterby fluid flow due to a spinning stretching disk with non-Fourier/Fick heat and mass flux models. *Applied Mathematics and Mechanics*, *42*(9), 1247–1258. https://doi.org/10.1007/s10483-021-2770-9
22. Abdal, S., Siddique, I., Afzal, S., Sharifi, S., Salimi, M., & Ahmadian, A. (2022). An analysis for variable physical properties involved in the nano-biofilm transportation of sutterby fluid across shrinking/stretching surface. *Nanomaterials*, *12*(4), 599. https://doi.org/10.3390/nano12040599
23. Hanif, A., Abbas, Z., & Khaliq, S. (2023). Rheological impact of Sutterby fluid in isothermal forward roll coating process: A theoretical study. *Journal of Plastic Film & Sheeting*, *39*(1), 115–133. https://doi.org/10.1177/87560879221111820
24. Hussain, I., Khan, W. A., Tabrez, M., & Irfan, M. (2023). Dynamics of stratifications and magnetic dipole for radiative flow of ferromagnetic Sutterby fluid. *ZAMM-Journal of Applied Mathematics and Mechanics/Zeitschrift Für Angewandte Mathematik Und Mechanik*, *103*(3): Article e202200226.
25. Abdelsalam, S. I., Magesh, A., Tamizharasi, P., & Zaher, A. Z. (2023). Versatile response of a Sutterby nanofluid under activation energy: Hyperthermia therapy. *International Journal of Numerical Methods for Heat & Fluid Flow*, *34*(2), 408–428. https://doi.org/10.1108/HFF-04-2023-0173
26. Daniel, Y. S., Aziz, Z. A., Ismail, Z., & Salah, F. (2017). Entropy analysis in electrical magnetohydrodynamic (MHD) flow of nanofluid with effects of thermal radiation, viscous dissipation, and chemical reaction. *Theoretical and Applied Mechanics Letters*, *7*(4), 235–242. https://doi.org/10.1016/j.taml.2017.06.003
27. Mulinti, V. R., & Pallavarapu, L. (2022). Influence of thermal radiation and viscous dissipation on MHD flow of UCM fluid over a porous stretching sheet with higher order chemical reaction, *Spec. Top Rev. Porous Media Int. J*, *12*(4), 2215–2233.
28. Wakif, A., Abderrahmane, A., Guedri, K., Bouallegue, B., Kaewthongrach, R., Kaewmesri, P., & Jirawattanapanit, A. (2022). Importance of exponentially falling variability in heat generation on chemically reactive von k′ arm′ an nanofluid flows subjected to a radial magnetic field and controlled locally by zero mass flux and convective heating conditions: A differential quadrature analysis. *Frontiers in Physics*, *10*, 768. https://doi.org/10.3389/fphy.2022.988275

29. Vinodkumar, M., Reddy., & P., Lakshminarayana. (2022). Higher order chemical reaction and radiation effects on magnetohydrodynamic flow of a maxwell nanofluid with Cattaneo–Christov heat flux model over a stretching sheet in a porous medium. *J. Fluid Eng*, *144*(4), 041204.
30. Yahaya, S. D., Aliyu, U., & Umaru, H. (2022). Stagnation point flow with thermal and magnetic field over a stretching sheet. *Scientific World Journal*, *17*(2), 191–199.
31. Mahabaleshwar, U. S., Sneha, K. N., & Wakif, A. (2023). Significance of Thermo-Diffusion and Chemical Reaction on MHD Casson Fluid Flows Conveying CNTs over a Porous Stretching Sheet. *Waves in Random and Complex Media*, (43), 1–19. https://doi.org/10.1080/17455030.2023.2173500
32. Anwar, M. I., Firdous, H., Zubaidi, A. A., Abbas, N., & Nadeem, S. (2022). Computational analysis of induced magnetohydrodynamic non-Newtonian nanofluid flow over nonlinear stretching sheet. *Prog. React. Kinet. Mech*, *47*, 14686783211072712.
33. Alkasasbeh, H. T., Abderrahmane, A., Mourad, A., Guedri, K., Tag, E. M., & Younis, O. (2023). Analysis of 3-D MHD maxwell hybrid nanofluid flow over a stretching sheet. *Heliyon*, *47*(1), 4376147. https://doi.org/10.2139/ssrn.4376147, 1–23.
34. Shahid, A., Huang, H. L., Bhatti, M. M., & Marin, M. (2022). Numerical computation of magnetized bioconvection nanofluid flow with temperature-dependent viscosity and Arrhenius kinetic. *Mathematics and Computers in Simulation*, *200*, 377–392. https://doi.org/10.1016/j.matcom.2022.04.032
35. Elboughdiri, N., Ghernaout, D., Muhammad, T., Alshehri, A., Sadat, R., Ali, M. R., & Wakif, A. (2023). Towards a novel EMHD dissipative stagnation point flow model for radiating copper-based ethylene glycol nanofluids: An unsteady two-dimensional homogeneous second-grade flow case study, *Case. Case Studies in Thermal Engineering*, *45*, 102914. https://doi.org/10.1016/j.csite.2023.102914
36. Bhavya, N. P., Gayathri, M. S., Dinesh, P. A., & Jyothirmayi, M. (2023). A Nanofluid Boundary Layer Flow Over a Stretching Body in the Presence of Porous Medium. *Journal of Mines, Metals and Fuels*, *71*(11), 2334–2341. https://doi.org/10.18311/jmmf/2023/36258
37. Khan, W. A., & Pop, I. (2010). Boundary-layer flow of a nanofluid past a stretching sheet. *International Journal of Heat and Mass Transfer*, *53*(11-12), 2477–2483. https://doi.org/10.1016/j.ijheatmasstransfer.2010.01.032